Got TiO_2 Nanotubes? Lithium Ion Intercalation Can Boost Their Photoelectrochemical Performance

Benjamin H. Meekins and Prashant V. Kamat*

Radiation Laboratory and Departments of Chemistry and Biochemistry, and Chemical and Biomolecular Engineering, University of Notre Dame, Notre Dame, Indiana 46556

ARTICLE

ABSTRACT Cations such as H^+ and Li^+ are intercalated into TiO_2 nanotube arrays by subjecting them to short-term electrochemical pulses at controlled potentials (< -1.0 V *vs* Ag/AgCl). The intercalation of these small cations has a profound effect toward enhancing photocurrent generation under UV light irradiation. A nearly three-fold increase in the photoconversion efficiency (IPCE) was observed upon intercalation of Li^+ ions into TiO_2 nanotube arrays. The intercalation process is visualized by the color change from gray to blue. Spectroelectrochemical measurements were carried out to monitor the absorption changes at different applied potentials. The analysis of the V_{oc} decay following termination of UV light shows a significant decrease in the rate of recombination of accumulated electrons upon Li^+ ion intercalation.

KEYWORDS: TiO_2 nanotubes · lithium ion intercalation · solar cells · photoelectrochemistry · electron traps

TiO_2 nanotube arrays prepared by anodic corrosion of Ti films are useful as 1-D scaffolds to anchor light-harvesting assemblies.[1−4] These TiO_2 nanotube arrays consist of 50−100 nm diameter and 1−100 μm long tubes and become crystalline upon annealing. Their application in batteries,[5−8] solar cells,[9−15] and sensors[16−19] has drawn significant interest from the research community. Although TiO_2 responds only in the UV, the photoresponse of these nanotubes can be extended into the visible by anchoring dye molecules and semiconductor quantum dots to the nanotube array. Recent studies from our group investigated quantum-dot-sensitized solar cells by modifying the TiO_2 nanotube surface with different size quantum dots.[9,13] As compared to the particulate films, the one-dimensional structures show significant enhancement in the photoelectrochemical performance because of improved charge collection efficiency.[12]

TiO_2 is a useful photocatalyst to induce oxidative transformations in both chemical[20−23] and biological reactions,[24] as a co-catalyst with other materials such as Au, Ag, Co, and Pt,[20−23,25−32] and in gas sensing applications.[33] Another focus of TiO_2 nanoarrays is in the generation of photocatalytic solar hydrogen production.[2] The TiO_2 tubular films exhibit improved photoconversion efficiency over particulate systems in splitting water under UV excitation. However, because of the limited spectral match of the solar spectrum (<5%), the overall photoconversion efficiency for these systems remains quite low (<1%). Another interesting property is the ability to intercalate cations into the TiO_2 lattice. For example, simultaneous photoaccumulation of electrons and protons in TiO_2 has been demonstrated using a quartz crystal microbalance.[34] Efforts have also been made to incorporate other ions such as Li^+ during the synthesis of TiO_2.[35] Harima *et al.* showed that Li^+ ions may enhance photoelectric performance in TiO_2 powders.[36]

The electron trapping processes in TiO_2 have been extensively studied in the literature.[37−40] A quantitative transfer of electrons to other nanostructures such as gold[31] and carbon nanotubes[41] has led to the determination of the Fermi level of heterostructures. As the electrons are captured by Ti^{4+} sites to form Ti^{3+}, cations from solution (*e.g.*, Li^+ or H^+) intercalate into TiO_2 to compensate for the loss of charge (Scheme 1). In a recent study, it has been shown that TiO_2 nanotubes under strong negative bias exhibit a large increase in both capacitance and conductivity, indicating Fermi level displacement.[42] Filling of such electron trap sites using an electrochemical reduction method should allow us to boost the photoelectrochemical performance of TiO_2 nanotube array electrodes.

In order to further exploit the trap state filling for improving the photoelec-

*Address correspondence to pkamat@nd.edu.

Received for review July 30, 2009 and accepted October 18, 2009.

Published online October 29, 2009.
10.1021/nn900897r CCC: $40.75

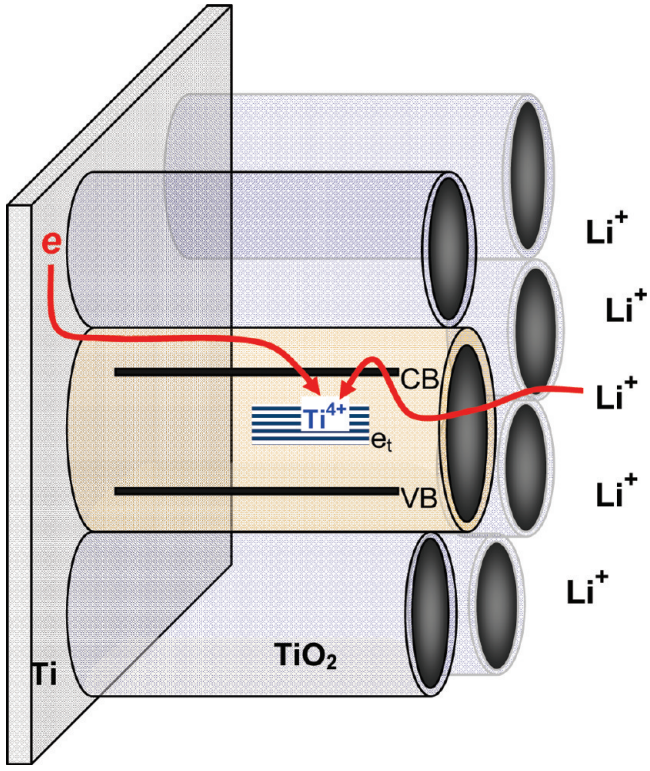

Scheme 1. Electrochemical conversion of Ti^{4+} to Ti^{3+} and simultaneous incorporation of Li^+ cations in TiO_2 nanotube array electrode.

trochemical performance, we have successfully intercalated lithium ions into TiO_2 nanotube arrays using an electrochemical approach. The optical properties of the Li^+-intercalated TiO_2 nanotube arrays and the effect of cation intercalation on the photocurrent generation are discussed.

RESULTS AND DISCUSSION

The anodic corrosion of a Ti film in a fluoride solution produces an ordered TiO_2 nanotube array. The diameter and length of the tubes can be varied by altering the medium and electrochemical corrosion conditions.[43] Figure 1A,C show scanning electron micrographs (SEM) of TiO_2 nanotubes as formed on a Ti substrate following the electrochemical etching and annealing procedure. The nanotube array showed a uniform distribution with a diameter in the range of 50−60 nm and length of ~5 μm.

The TiO_2 nanotube array electrode was subjected to electrochemical pulsing in a 3-arm electrochemical cell containing aqueous solution of 1 M perchlorate with different cations (H^+, Li^+, or TBA^+), a Pt counter electrode, and a Ag/AgCl reference electrode. A potential of −1.5 V voltage was applied for 3 s. During this short duration of applied electrochemical potential, the Ti^{4+} sites within the TiO_2 array get reduced to Ti^{3+}. In order to compensate for the lost charge, the cations from

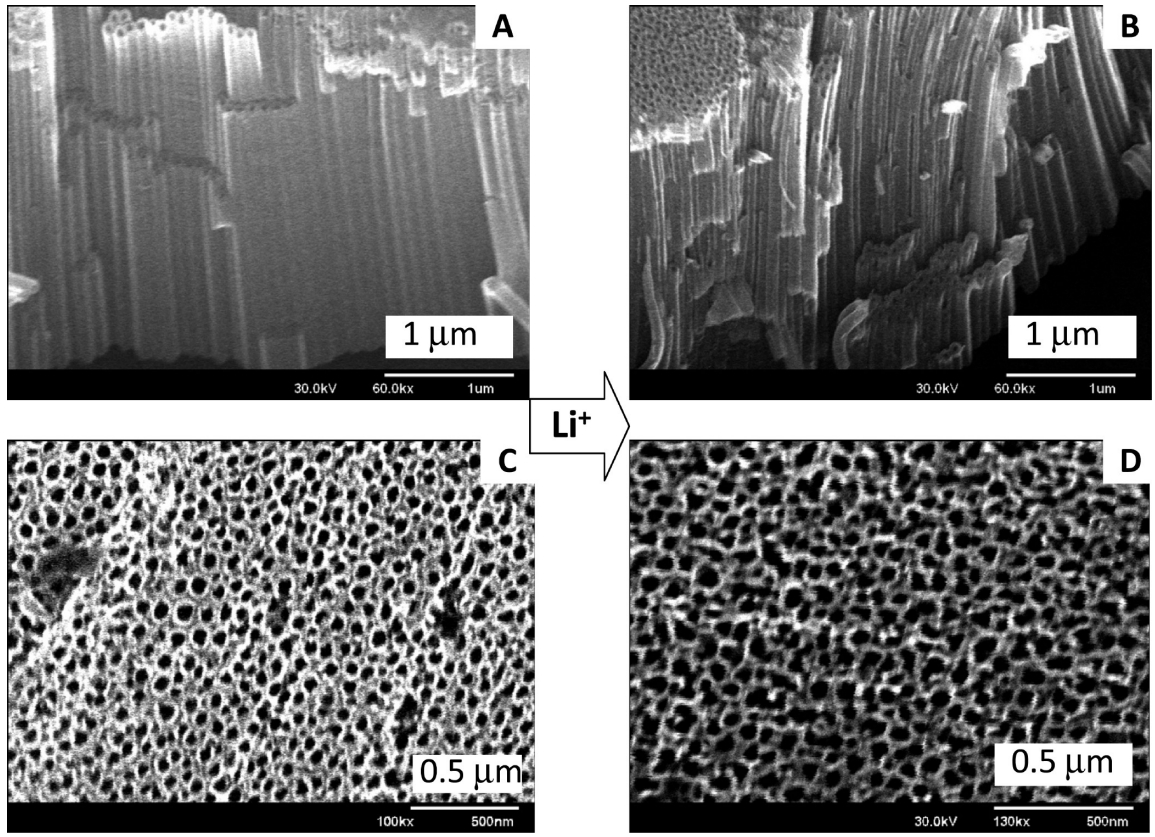

Figure 1. SEM images of TiO_2 nanotube array formed on Ti substrate using anodic etching procedure: profile of tubes (A) before Li^+ intercalation and (B) after Li^+ intercalation. Top-down view of tubes (C) before Li^+ intercalation and (D) after Li^+ intercalation.

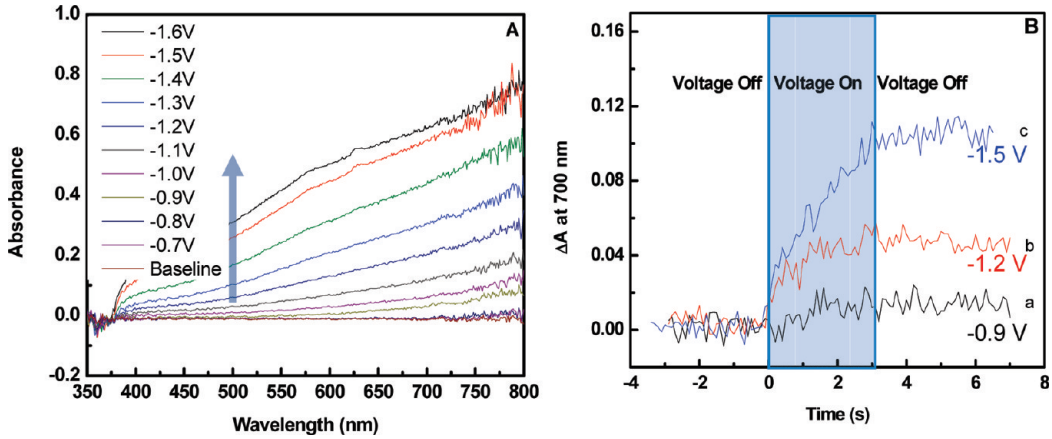

Figure 2. (A) Diffuse reflectance spectra of TiO_2 nanotube array after maintaining the electrode at a set potential for 3 s using a spectroelectrochemical setup (electrolyte: aqueous solution of 1 M $LiClO_4$, Ag/AgCl reference electrode, and Pt counter electrode). (B) Response of transient absorbance at 700 nm to applied potentials: (a) −0.9 V, (b) −1.2 V, and (c) −1.5 V in 1 M $LiClO_4$ electrolyte.

the solution (*e.g.*, H^+ or Li^+) intercalate within the TiO_2 lattice. Figure 1B,D show two different views of Li^+-intercalated TiO_2 nanotubes following the application of −1.5 V in a $LiClO_4$ medium. Comparison of the SEM figures in Figure 1 shows that the intercalation of cations such as Li^+ ions causes relatively little change in the overall morphology of the TiO_2 nanotube array.

The reduction of Ti^{4+} to Ti^{3+} states in TiO_2 is accompanied by a change in color from gray to a dark blue. For example, TiO_2 colloids prepared in ethanol undergo blue coloration when subjected to UV irradiation as electrons are accumulated at Ti^{4+} sites.[44] In a complementary procedure, electrochemical reduction is also known to induce electrochromic effects.[45] Electron paramagnetic resonance (EPR) and transient absorption studies have been performed to establish the nature of Ti^{3+} sites in TiO_2.[46−49] The accumulation of photogenerated electrons usually occurs at shallow traps (Ti^{4+} sites). The accessibility of these trapped electrons for secondary electron transfer to an acceptor molecule (*e.g.*, O_2, C_{60}, and methyl viologen)[44,50,51] or electrode[52,53] shows the reversibility of the trapping process. The electrochemical reduction, on the other hand, can lead to the filling of both shallow and deep traps. If the electrode is subjected to electrochemical potential more negative than −1.0 V *vs* Ag/AgCl, the color changes remain stable as the intercalation of cations brings in charge compensation.

No lasting change in the absorption is seen at potentials less than −1.1 V *vs* Ag/AgCl with 1 M $LiClO_4$ as the electrolyte. As the electrode is maintained at potentials more negative than −1.0 V *vs* Ag/AgCl, we observe broad absorption in the red and infrared region (Figure 2A). These changes in the absorption represent reduction of Ti^{4+} sites to Ti^{3+} sites and the accompanying intercalation of cations. The growth of peak absorbance, which corresponds to the maximum absorbance observed at the end of the 3 s potential pulse, for Li^+ cations is summarized in Figure 2B. The growth of absorption is promptly seen during the application of electrochemical potential and attains a maximum within the duration of the pulse.

In order to see the influence of other cations, we also conducted the spectroelectrochemical measurements using 1 M tetrabutylammonium perchlorate (TBAP) in 1 M $HClO_4$. The dependence of steady state absorbance on applied potential for H^+ and Li^+ cations is shown in Figure 3A. The absorbance at 700 nm was monitored following the application of 3 s potential pulse until it attained a steady absorbance value. Figure 3A shows that the stability of Ti^{3+} states can be seen at an onset potential of −1.1 V when Li^+ ions are present in solution. With increasing negative potential, this steady state absorbance increases, attaining a plateau at −1.8 V. This value represents an upper limit when all the available Ti^{4+} sites are converted to Ti^{3+} sites. A similar trend is also seen when Li^+ ions are replaced by H^+ ions; however, a positive shift of ~0.6 V in the onset potential is seen because of the change in the pH as well as the size of the cation. It is well-established that the band edges of TiO_2 shift to positive potentials (0.059 V/pH unit) with decreasing pH.[54] A shift of the conduction band to more positive potential in $HClO_4$ allows the transformation of Ti^{4+} to Ti^{3+} to occur at a lower onset potential. This potential for intercalation of H^+ ions is so low that the process can even be initiated with band gap excitation of TiO_2 in acidic medium.[42] It is interesting to note that both H^+ and Li^+ intercalate into TiO_2 to stabilize the Ti^{3+} sites in a similar fashion. The larger tetrabutylammonium ions, however, have no effect in inducing coloration. It is apparent that these large cations are unable to penetrate the lattice and stabilize Ti^{3+} sites.

Another interesting aspect is the stability of the as-formed Ti^{3+} sites when intercalation was carried out with Li^+ ions. Figure 3B shows that Ti^{3+} generated during the application of electrochemical potential pulse remains stable even upon application of more positive

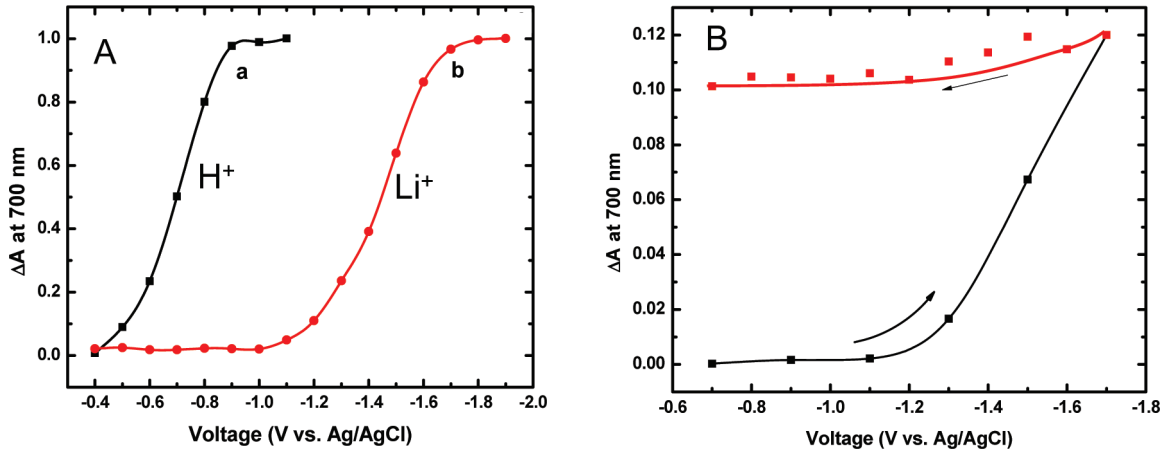

Figure 3. (A) Normalized growth of steady state absorption at 700 nm at different applied potentials in 1 M electrolytes: (a) $HClO_4$ and (b) $LiClO_4$. The maximum absorbance was normalized to 1.0. (B) Steady state absorption at 700 nm at different applied potentials (electrolyte: 1 M $LiClO_4$) during forward (black squares) and reverse (red squares) cycles.

potentials. Sodergren[55] found that Li^+ ions intercalated into a nanoporous anatase TiO_2 film by applying a −1.7 V *vs* Ag/AgCl for 5 min. The intercalation in these experiments could easily be reversed by applying a −0.15 V *vs* Ag/AgCl for 5 min. Even at applied potentials of 0 and +0.2 V *vs* Ag/AgCl for 5 min, we observed little change in absorbance. Less than 25% decrease in the absorbance was observed upon application of +1.0 V *vs* Ag/AgCl (see Supporting Information). It is not apparent why there is such a large discrepancy of reversibility between the nanoporous TiO_2 (see ref 55) and the TiO_2 nanotubes employed in our work. It should be noted that TiO_2 nanotube-based Li-ion batteries exhibit reversibility in the range of 75−90%,[5] and hence, some irreversibility persists in these systems. Variation in preparative methods and the nature of trap states are likely to contribute to the difference in behavior with respect to reversibility. We have performed XRD measurements to probe changes in crystalline phase following the intercalation of Li^+ ions. The results presented in the Supporting Information (Figure S2) rule out such a possibility. On the basis of these results, we can conclude that the parent rutile structure is retained following Li^+ intercalation.

Effect of Cation Intercalation on the Photoelectrochemical Behavior of TiO_2 Nanotube Array Electrode. The effect of the H^+ and Li^+ intercalation on the photoelectrochemical properties of the TiO_2 nanotube electrode was studied in a 3-arm electrochemical cell. The current response to on−off cycles of UV illumination ($\lambda > 310$ nm) was recorded by maintaining an electrode potential at 0 V *vs* Ag/AgCl in 1 M KOH. As can be seen in Figure 4A, the photocurrent response to UV illumination in both cases was prompt and reproducible. The TiO_2 nanotube array electrodes subjected to electrochemical bias treatment (−1.5 V, 3 s pulse) exhibit higher photocurrent than those without any treatment. These results indicate the beneficial role of cation intercalation in improving the photocurrent generation at the TiO_2 nanotube electrode. Intercalation of Li^+ ions yields higher photo-

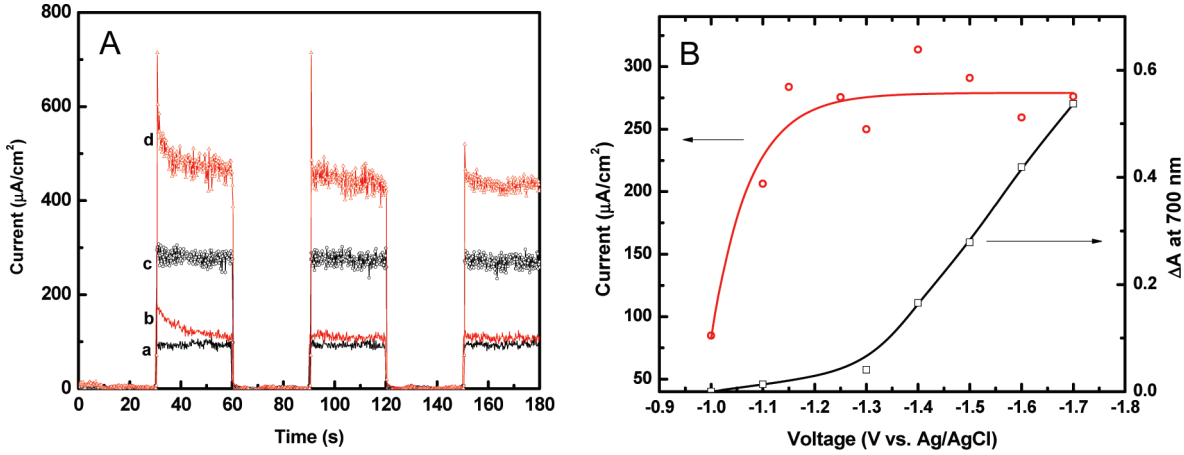

Figure 4. (A) Photocurrent response of TiO_2 nanotube array before (a,b) and after (c,d) the electrochemical treatment in 1 M solutions of $HClO_4$ (a,c) and $LiClO_4$ (b,d) to on−off cycles of UV illumination. Electrolyte was 1 M KOH. (B) Changes in steady state photocurrent and absorbance at 700 nm under UV illumination (1 M KOH electrolyte) *vs* applied voltage. A 3 s pulse at a set voltage was applied using 1 M $LiClO_4$ prior to each measurement. After each pulse, the nanotube array electrode was allowed to sit overnight before the photocurrent measurements.

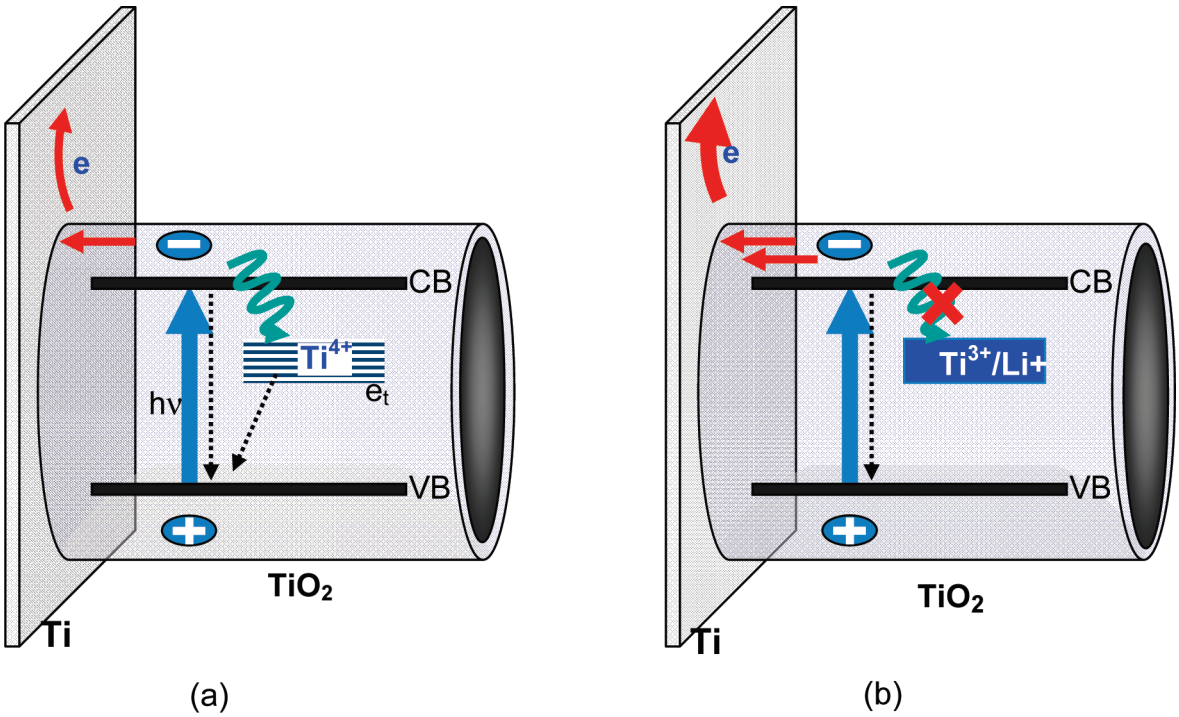

Scheme 2. Band energy diagram showing the charge separation, electron trapping at Ti^{4+} sites, and electron transport to Ti substrate in (a) a pristine TiO_2 nanotube and (b) a partially reduced TiO_2 nanotube with Li^+ intercalation. Blocking of electron trapping in (b) enhances the possibility of electron capture for photocurrent generation.

current than electrodes intercalated with H^+ ions. The nearly three-fold enhancement seen following Li^+ ion intercalation reveals a simple way to boost the photoelectrochemical activity of TiO_2 nanotubes.

Li^+ ion intercalation has been widely used to develop storage batteries.[5,56] In these applications, Li^+ ion intercalation is expected to show reversibility as the electrode is subjected to charge−discharge cycles. Several studies show only a partial degree of reversibility toward Li^+ ion release when nanostructured TiO_2 is used as the storage electrode.[5,57,58] Earlier studies with TiO_2 particulate films showed reversibility of Li^+ ion intercalation from the change in the blue coloration.[57,59] In the present study, we employed a more negative potential, −1.5 V *vs* Ag/AgCl, that facilitated intercalation of deeper sites within the TiO_2 nanotubes. The fact that these electrodes continue to deliver stable photocurrents for repeated on−off illumination cycles further supports the argument that the Li^+ ions are strongly intercalated into TiO_2 nanotubes. We also did not observe any decrease in coloration of the TiO_2 nanotube electrode or decrease in photocurrent following continuous illumination of the electrode at 0 V *vs* Ag/AgCl for 15 min.

Figure 4B shows the dependence of maximum photocurrent of TiO_2 nanotube array electrode and its absorbance at 700 nm on the applied electrochemical potential. The TiO_2 nanotube array electrode was subjected to a given potential for 3 s in an electrochemical cell while recording the absorbance until steady state was attained. The electrode was then washed and allowed to rest overnight before recording photocurrent values. When TiO_2 nanotube arrays are pretreated with electrochemical bias at potentials less negative than −1.0 V, one does not observe any noticeable change in the photocurrent generation or absorbance. A steep rise in the photocurrent could be seen for TiO_2 nanotube array electrodes that were pretreated with electrochemical pulse in the range of −1.0 to −1.2 V. Under the same conditions, we see only a small increase in the 700 nm absorption indicating the reduction of Ti^{4+} sites and Li^+ intercalation. The absorbance at 700 nm continues to show a rise when we apply more negative potentials; there is, however, no significant increase in the photocurrent at potentials more negative than −1.2 V. As shown earlier, Ti^{4+} sites usually act as electron traps, and the trapped electrons can survive for a long period of time.[37−40] During the application of negative potential, one expects filling of electron traps, thus making these sites unavailable for trapping photogenerated electrons (Scheme 2). On the basis of the results in Figure 4B, we can conclude that the filling of shallow traps at lower applied potentials (−1.2 V) is sufficient to attain amplification in the photocurrent generation. At more negative potentials, the deeper traps get filled but this process does not seem to have any noticeable effect on the photocurrent generation.

Photoconversion Efficiency. That the photocurrent originates only from UV excitation is further borne out by photocurrent action spectra. Incident photon to charge carrier generation efficiency—IPCE (also referred to as

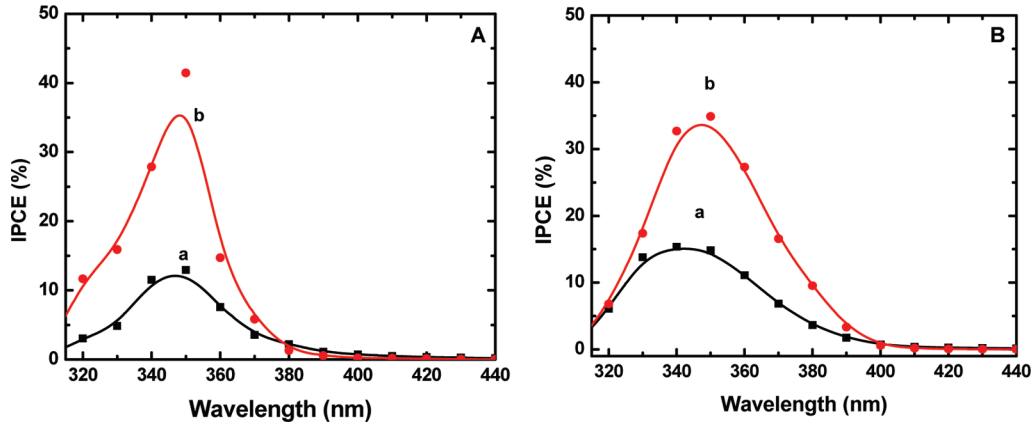

Figure 5. A) IPCE (%) of the TiO_2 nanotube array electrode: (a) before and (b) after Li^+ intercalation. (B) IPCE (%) of the TiO_2 nanotube electrode (a) before and (b) after H^+ intercalation. Electrolyte in all experiments was 1 M KOH.

external quantum efficiency)—values at different light wavelengths were determined from eq 1

$$\text{IPCE}(\%) = \frac{1240}{\lambda}\frac{i_{sc}}{I_{inc}} \times 100\% \qquad (1)$$

where λ refers to wavelength in nm, i_{sc} refers to short circuit current in mA/cm^2, and I_{inc} refers to the power of the incident light in mW/cm^2. As can be seen from Figure 5, the onset of photocurrent for both sets of experiments is similar. The onset potential seen around 380 nm corresponds to the band gap transition of 3.2 eV and confirms that the band gap transition is unaffected by Li^+ ion intercalation. The TiO_2 nanotube array electrode does not respond to visible light excitation. Despite the blue coloration of the Li^+-ion-intercalated TiO_2 nanotubes, these color centers have no direct role in the photoinduced charge separation. Hence, we attribute the indirect influence of Li^+ ion intercalation in boosting the IPCE to the blocking of charge recombination sites within the TiO_2 lattice.

The maximum IPCE seen for the untreated TiO_2 nanotube array at 350 nm is around 12%, while the Li^+-ion-intercalated electrode exhibits an IPCE of 42%, a nearly 3.5-fold enhancement. H^+-intercalated TiO_2, on the other hand, only gives a 2-fold enhancement of IPCE, as seen in Figure 5B. At excitations below 350 nm, we observed a decrease in the IPCE as light absorption throughout the TiO_2 nanotube array becomes non-uniform. Because of the large absorption cross section of TiO_2 at shorter wavelengths, most of the incident light is absorbed near the outer surface. It should be noted that the IPCE results presented here were obtained without any external bias. The higher IPCE value reported in the literature (80%) employs external bias to suppress charge recombination and facilitate electron transport within the TiO_2 film.[60] For the deployment of a practical solar cell, it is important to evaluate efficiency values using a two-electrode configuration (without external bias).

***I*−*V* Characteristics.** In order to see the effect of intercalation of different cations, we recorded current−voltage (*I*−*V*) plots using a three-electrode setup. The *I*−*V* plots of the TiO_2 nanotube array electrodes before and after cation intercalation are shown in Figure 6. These experiments were carried out using a 2 mV/s voltage scan rate. The TiO_2 nanotube array electrode before and after Li^+ ion intercalation retains the fundamental property of generating anodic photocurrent but with different magnitudes (Figure 6). An increase in the overall efficiency of the TiO_2 nanotube array electrode is seen with both H^+ and Li^+ ion intercalation—approximately double with H^+ and approximately triple with Li^+. The shift in the flat-band potential, as monitored from the zero current potential, shows a small negative shift (20−50 mV) as a result of the cation intercalation. This shift in flat-band potential is consistent

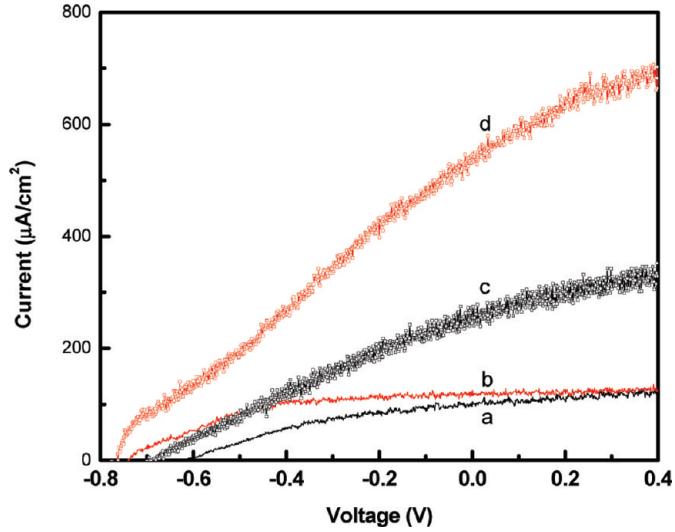

Figure 6. Current−voltage characteristics of two separate TiO_2 nanotube array electrodes: (a,b) before and (c,d) after subjecting them to electrochemical bias. The counterions (c) H^+ and (d) Li^+ were intercalated by applying 3 s pulse at −1.5 V. Electrolyte was 1 M KOH. Reference was Ag/AgCl (saturated KCl). Scan direction was from negative to positive potentials at a scan rate of 2 mV/s.

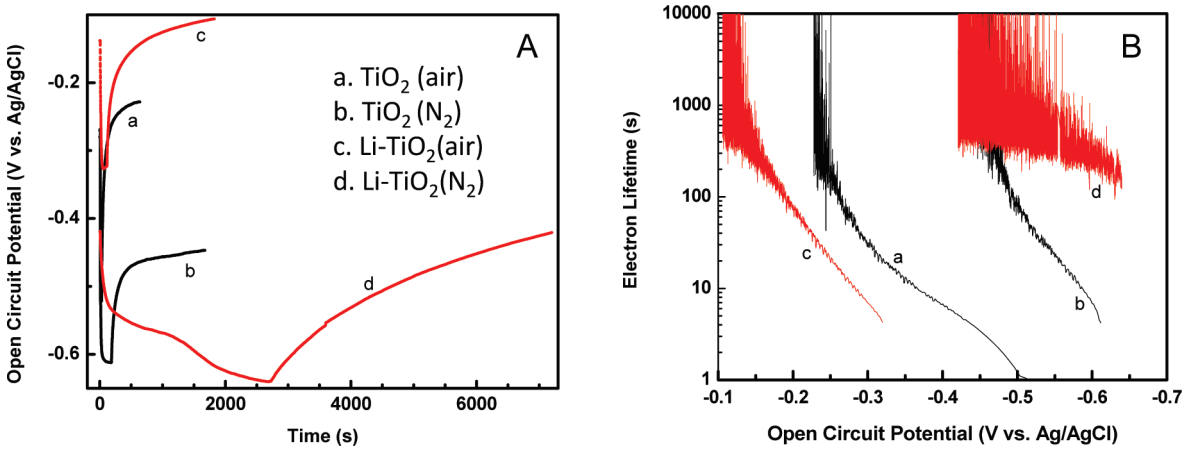

Figure 7. (A) V_{oc} time profile of TiO_2 nanotube arrays (a,b) before and (c,d) after intercalation of Li^+ ions in the (a,c) air-equilibrated and (b,d) nitrogen-saturated 1 M KOH solution. The illumination was terminated after attaining a steady V_{oc}. (B) Electron lifetime measurements determined from the V_{oc} decay in dark as analyzed from traces in panel A and eq 2.

with the hypothesis that the cation intercalation leads to unpinning of the Fermi level and gets closer to the conduction band.[42] These results further confirm the beneficial effects of blocking of trap sites with electrochemical reduction of Ti^{4+} and intercalation with cations in improving overall photoelectrochemical performance of the TiO_2 nanotube array electrode.

Electron Accumulation and Decay Lifetimes. It is evident from the photocurrent measurements that the reduction of Ti^{4+} sites paired with Li^+ intercalation improves the photoelectrochemical performance of TiO_2 nanotube arrays. If indeed the observed improvement in the photoconversion efficiency (Figure 5) is the result of blocking of electron trap sites, we should be able to suppress the charge recombination at the trap sites. In order to probe the electron accumulation and its susceptibility to charge recombination, we monitored the photovoltage and its decay upon termination of illumination. The relationship between the photovoltage decay and electron disappearance in TiO_2 has recently been established by infrared spectroscopy.[61,62]

Figure 7A shows a typical open-circuit voltage response (V_{oc}) to illumination followed by termination of illumination. The open-circuit voltage of the photoelectrochemical cell represents the difference in Fermi level between the TiO_2 and counter electrodes. In the dark, the electrode potential is dictated by redox equilibration. Band gap excitation of TiO_2 results in charge separation. As the holes are scavenged by OH^- at the interface, the electrons begin accumulating within the TiO_2 film. Electron accumulation causes a shift of the Fermi level to more negative potentials, and we see an increase in V_{oc}. The open-circuit voltage reaches a maximum as the electron accumulation competes with the charge recombination and thus attains a steady state. Upon stopping the illumination, V_{oc} decays as the electrons accumulated within the TiO_2 are scavenged by the electron acceptor species in the electrolyte (*e.g.*, dissolved oxygen) as well as undergo recombination with trapped holes. Thus, monitoring the decay of the voltage provides an insight into the pathways by which loss of accumulated electrons occurs within the TiO_2 network.

The open-circuit voltage after stopping the UV illumination exhibits a complex decay and can be analyzed using the approximation derived by Bisquert.[63] According to this model, the decay lifetime of the accumulated electrons can be related to the drop in potential using eq 2

$$\tau = \frac{k_B T}{e}\left(\frac{dV_{oc}}{dt}\right)^{-1} \quad (2)$$

where τ is the potential dependent lifetime, k_B is Boltzmann's constant, T is the temperature in K, e is the charge of a single electron, and V_{oc} is the open-circuit voltage at time t. The electron lifetimes determined with eq 2 were compared in the presence and absence (N_2-purged) of oxygen in the electrolyte. The relationship between the lifetime of electrons in TiO_2 nanotubes and the V_{oc} is presented in Figure 7B. The range of lifetimes recorded for TiO_2 nanotubes presents two interesting observations. First, the V_{oc} exhibits a rapid decrease when oxygen is present in the electrolyte both before and after Li^+ intercalation of the TiO_2 nanotubes. Second, the electron lifetime in N_2-purged solutions is significantly longer. In particular, Li^+-intercalated TiO_2 nanotubes exhibit a significant increase in the electron lifetime in the absence of oxygen.

Surface traps play an important role in electron accumulation and transport across the nanostructured TiO_2 film. In DSSCs, charge recombination within the TiO_2 particle is not a major issue because only photoinjected electrons are accumulated inside the particle. These accumulated electrons are lost at the interface *via* recombination with redox couples such as I_3^-. In the present experiments, we are subjecting TiO_2 nanotubes to direct band gap excitation, and both trapped electrons and trapped holes remain within the particle.

The trap-mediated recombination processes are slower compared to direct electron−hole recombination. Although we remove a fraction of deep traps responsible for charge recombination, other surface traps still remain. This is evident from the long lifetime of voltage decay in the absence of O_2. Such traps beneficially facilitate transport of electrons in the TiO_2 film.

The results presented in this work point out the beneficial role of Li^+ intercalation in stabilizing photogenerated electrons. In the absence of surface-adsorbed scavengers such as O_2, the electrons survive for a longer period of time as the surface defects are blocked as a result of the Li^+ intercalation. Such improved TiO_2 nanostructures are potentially useful in boosting the performance of dye-sensitized or quantum-dot-sensitized solar cells. Efforts are currently underway to test the photocatalytic activity of these materials in solar hydrogen production.

CONCLUSIONS

Cations such as H^+ and Li^+ readily intercalate into TiO_2 nanotubes when subjected to negative bias. The reduction of Ti^{4+} sites by electrons and simultaneous intercalation of cations alter the properties of TiO_2 nanotubes. A three-fold increase in both photocurrent generation and IPCE was observed with the TiO_2 nanotube array electrodes previously subjected to an electrochemical bias (−1.5 V *vs* Ag/AgCl in 1 M $LiClO_4$ for 3 s). A small shift in the flat-band potential was also evident as a result of the unpinning of the Fermi level as we intercalated cations into TiO_2 nanotubes. The increase in the electron lifetime in the absence of oxygen was confirmed from the decay of the open-circuit potential after stopping the UV illumination.

EXPERIMENTAL SECTION

Materials and Preparation. Ti foil (0.25 mm, 99.7% purity) was purchased from Alfa Aesar. The foils were cut into 4 cm × 0.8 cm pieces, sonicated in 2-propanol, and stored in acetone until used. Ammonium fluoride and lithium perchlorate were purchased from Sigma Aldrich and used as received. Potassium hydroxide pellets were purchased from Fisher Scientific and used as received. Tetrabutylammonium perchlorate (TBAP) was purchased from Alfa Products and used as received.

TiO_2 nanotubes were prepared using a standard electrochemical anodizing process.[43] Ti foil was anodized at 60 V in a mixture of ethylene glycol (98% w/v)/water (2% w/v) containing 0.27 M ammonium fluoride for 1.5 h. This procedure produced nanotubes with lengths ranging from 5 to 10 μm and diameters of approximately 50 to 60 nm. After anodization, the foils were sonicated for 1−5 s, rinsed in water, dried in an air stream, and annealed at 450 °C for 3 h, with a 1 °C/min ramp rate.

The cation intercalation of the TiO_2 nanotube array electrode was carried out in a 3-arm electrochemical cell. The TiO_2 nanotube array served as the working electrode. Either 1 M $HClO_4$ or 1 M $LiClO_4$ was used as the electrolyte for cation intercalation, while a platinum mesh served as a counter electrode and Ag/AgCl (saturated KCl) as a reference electrode. A potential of −1.5 V (*vs* Ag/AgCl) was applied for 3 s, according to the best result obtained by Macak and Schmuki.[64] A color change to dark blue provided visual confirmation of the reduction of Ti^{4+} to Ti^{3+} and simultaneous intercalation of cations. The electrode was removed, washed with deionized water, dried under an air stream, and allowed to rest overnight before photoelectrochemical measurements were made.

Characterization. Photoelectrochemical measurements were made using a Princeton Applied Research PARstat 2273 potentiostat and a three-electrode setup with a platinum counter electrode and KCl-saturated Ag/AgCl reference electrode. Nitrogen was bubbled for several minutes before experiments were started and allowed to flow over the surface of the electrolyte to prevent reentry of air. A 300 W xenon white light source with >310 nm $CuSO_4$ filter was used in all experiments. IPCE measurements were carried out in a two-electrode setup using a Keithley 617 programmable electrometer and a Bausch and Lomb high intensity monochromator with ~15 nm fwhm with no applied bias. One molar KOH was used as the electrolyte in both setups. Diffuse reflectance measurements were made using a Shimadzu UV-3101PC spectrophotometer. A white paper background was used as the reference. SEM pictures were taken with a Hitachi S-4500 FESEM.

Spectroelectrochemical measurements were carried out with a 3-arm cell inserted in the sample compartment of the spectrophotometer. Diffuse reflectance spectroscopy was used to monitor the absorption changes of the TiO_2 nanotube array electrode during and after completion of intercalation at different applied potentials. The TiO_2 nanotube array before the treatment served as reference to record the baseline. The voltage was varied from −0.4 to −1.8 V in −0.1 V increments with pulse duration of 3 s at each applied potential step; absorption spectra were recorded immediately following each potential pulse. Transient absorption spectra were also recorded at 700 nm to determine the steady state absorbance after each applied potential step.

X-ray diffraction (XRD) measurements were carried out with a Scintag X1 Advanced Diffraction System.

Acknowledgment. The research described herein was supported by the Department of Energy, Office of Basic Energy Sciences. This is contribution number NDRL 4821 from the Notre Dame Radiation Laboratory.

Supporting Information Available: Stability of intercalation as monitored from the absorption at 700 nm and XRD spectra are provided. This material is available free of charge *via* the Internet at http://pubs.acs.org.

REFERENCES AND NOTES

1. Kamat, P. V. Quantum Dot Solar Cells. Semiconductor Nanocrystals as Light Harvesters. *J. Phys. Chem. C* **2008**, *112*, 18737–18753.
2. Shankar, K.; Basham, J. I.; Allam, N. K.; Varghese, O. K.; Mor, G. K.; Feng, X.; Paulose, M.; Seabold, J. A.; Choi, K.-S.; Grimes, C. A. Recent Advances in the Use of TiO_2 Nanotube and Nanowire Arrays for Oxidative Photoelectrochemistry. *J. Phys. Chem. C* **2009**, *113*, 6327–6359.
3. Macak, J. M.; Tsuchiya, H.; Ghicov, A.; Schmuki, P. Dye-Sensitized Anodic TiO_2 Nanotubes. *Electrochem. Commun.* **2005**, *7*, 1133–1137.
4. Albu, S. R.; Kim, D.; Schmuki, P. Growth of Aligned TiO_2 Bamboo-Type Nanotubes and Highly Ordered Nanolace. *Angew. Chem., Int. Ed.* **2008**, *47*, 1916–1919.
5. Ortiz, G. F.; Hanzu, I.; Djenizian, T.; Lavela, P.; Tirado, J. L.; Knauth, P. Alternative Li-Ion Battery Electrode Based on Self-Organized Titania Nanotubes. *Chem. Mater.* **2009**, *21*, 63–67.
6. Yoon, S.; Ka, B. H.; Lee, C.; Park, M.; Oh, S. M. Preparation of Nanotube TiO_2−Carbon Composite and Its Anode Performance in Lithium-Ion Batteries. *Electrochem. Solid State Lett.* **2009**, *12*, A28–A32.

7. Kim, S. W.; Han, T. H.; Kim, J.; Gwon, H.; Moon, H. S.; Kang, S. W.; Kim, S. O.; Kang, K. Fabrication and Electrochemical Characterization of TiO_2 Three-Dimensional Nanonetwork Based on Peptide Assembly. *ACS Nano* **2009**, *3*, 1085–1090.
8. Zhou, Y. K.; Cao, L.; Zhang, F. B.; He, B. L.; Li, H. L. Lithium Insertion into TiO_2 Nanotube Prepared by the Hydrothermal Process. *J. Electrochem. Soc.* **2003**, *150*, A1246–A1249.
9. Baker, D. R.; Kamat, P. V. Photosensitization of TiO_2 Nanostructures with CdS Quantum Dots. Particulate *versus* Tubular Support Architectures. *Adv. Funct. Mater.* **2009**, *19*, 805–811.
10. Wang, D. A.; Liu, Y.; Wang, C. W.; Zhou, F.; Liu, W. M. Highly Flexible Coaxial Nanohybrids Made from Porous TiO_2 Nanotubes. *ACS Nano* **2009**, *3*, 1249–1257.
11. Kuang, D.; Brillet, J.; Chen, P.; Takata, M.; Uchida, S.; Miura, H.; Sumioka, K.; Zakeeruddin, S. M.; Gratzel, M. Application of Highly Ordered TiO_2 Nanotube Arrays in Flexible Dye-Sensitized Solar Cells. *ACS Nano* **2008**, *2*, 1113–1116.
12. Zhu, K.; Neale, N. R.; Miedaner, A.; Frank, A. J. Enhanced Charge-Collection Efficiencies and Light Scattering in Dye-Sensitized Solar Cells Using Oriented TiO_2 Nanotubes Arrays. *Nano Lett.* **2007**, *7*, 69–74.
13. Kongkanand, A.; Tvrdy, K.; Takechi, K.; Kuno, M. K.; Kamat, P. V. Quantum Dot Solar Cells. Tuning Photoresponse through Size and Shape Control of CdSe−TiO_2 Architecture. *J. Am. Chem. Soc.* **2008**, *130*, 4007–4015.
14. Mor, G. K.; Shankar, K.; Paulose, M.; Varghese, O. K.; Grimes, C. A. Use of Highly-Ordered TiO_2 Nanotube Arrays in Dye-Sensitized Solar Cells. *Nano Lett.* **2006**, *6*, 215–218.
15. Jennings, J. R.; Ghicov, A.; Peter, L. M.; Schmuki, P.; Walker, A. B. Dye-Sensitized Solar Cells Based on Oriented TiO_2 Nanotube Arrays: Transport, Trapping, and Transfer of Electrons. *J. Am. Chem. Soc.* **2008**, *130*, 13364–13372.
16. Li, Z. Y.; Zhang, H. N.; Zheng, W.; Wang, W.; Huang, H. M.; Wang, C.; MacDiarmid, A. G.; Wei, Y. Highly Sensitive and Stable Humidity Nanosensors Based on LiCl Doped TiO_2 Electrospun Nanofibers. *J. Am. Chem. Soc.* **2008**, *130*, 5036–5037.
17. Bao, S. J.; Li, C. M.; Zang, J. F.; Cui, X. Q.; Qiao, Y.; Guo, J. New Nanostructured TiO_2 for Direct Electrochemistry and Glucose Sensor Applications. *Adv. Funct. Mater.* **2008**, *18*, 591–599.
18. Zheng, Q.; Zhou, B. X.; Bai, J.; Li, L. H.; Jin, Z. J.; Zhang, J. L.; Li, J. H.; Liu, Y. B.; Cai, W. M.; Zhu, X. Y. Self-Organized TiO_2 Nanotube Array Sensor for the Determination of Chemical Oxygen Demand. *Adv. Mater.* **2008**, *20*, 1044–1049.
19. Gong, D.; Grimes, C. A.; Varghese, O. K.; Hu, W. C.; Singh, R. S.; Chen, Z.; Dickey, E. C. Titanium Oxide Nanotube Arrays Prepared by Anodic Oxidation. *J. Mater. Res.* **2001**, *16*, 3331–3334.
20. George, P. P.; Gedanken, A.; Perkas, N.; Zhong, Z. Selective Oxidation of CO in the Presence of Air over Gold-Based Catalysts Au/TiO_2/C (Sonochemistry) and Au/TiO_2/C (Microwave). *Ultrason. Sonochem.* **2008**, *15*, 539–547.
21. Jasin, D.; Abu-Rabi, A.; Mentus, S.; Jovanovic, D. Oxygen Reduction Reaction on Spontaneously and Potentiodynamically Formed Au/TiO_2 Composite Surfaces. *Electrochim. Acta* **2007**, *52*, 4581–4588.
22. Rodriguez-Gonzalez, V.; Zanellac, R.; del Angela, G.; Gomeza, R. MTBE Visible-Light Photocatalytic Decomposition over Au/TiO_2 and Au/TiO_2-Al_2O_3 Sol−Gel Prepared Catalysts. *J. Mol. Catal A* **2008**, *281*, 93–98.
23. Paramasivalm, I.; Macak, J. M.; Schmuki, P. Photocatalytic Activity of TiO_2-Nanotube Layers Loaded with Ag and Au Nanoparticles. *Electrochem. Commun.* **2008**, *10*, 71–75.
24. Armelao, L.; Barreca, D.; Bottaro, G.; Gasparotto, A.; Maccato, C.; Maragno, C.; Tondello, E.; Stangar, U. L.; Bergant, M.; Mahne, D. Photocatalytic and Antibacterial Activity of TiO_2 and Au/TiO_2 Nanosystems. *Nanotechnology* **2007**, *18*, 375709.
25. Chen, M. S.; Goodman, D. W. Catalytically Active Gold on Ordered Titania Supports. *Chem. Soc. Rev.* **2008**, *37*, 1860–1870.
26. Dawson, A.; Kamat, P. V. Semiconductor−Metal Nanocomposites. Photoinduced Fusion and Photocatalysis of Gold-Capped TiO_2 (TiO_2/Au) Nanoparticles. *J. Phys. Chem. B* **2001**, *105*, 960–966.
27. Iliev, V.; Tomova, D.; Todorovska, R.; Oliver, D.; Petrov, L.; Todorovsky, D.; Uzunova-Bujnova, M. Photocatalytic Properties of TiO_2 Modified with Gold Nanoparticles in the Degradation of Oxalic Acid in Aqueous Solution. *Appl. Catal., A* **2006**, *313*, 115–121.
28. Kiyonaga, T.; Mitsui, T.; Torikoshi, M.; Takekawa, M.; Soejima, T.; Tada, H. Ultrafast Photosynthetic Reduction of Elemental Sulfur by Au Nanoparticle-Loaded TiO_2. *J. Phys. Chem. B* **2006**, *110*, 10771–10778.
29. Lopez, T.; Hernandez-Ventura, J.; Gomez, R.; Tzompantzi, F.; Sanchez, E.; Bokhimi, X.; Garcia, A. Photodecomposition of 2,4-Dinitroaniline on Li/TiO_2 and Rb/TiO_2 Nanocrystallite Sol−Gel Derived Catalysts. *J. Mol. Catal. A* **2001**, *167*, 101−107.
30. Mrowetz, M.; Villa, A.; Prati, L.; Selli, E. Effects of Au Nanoparticles on TiO_2 in the Photocatalytic Degradation of an Azo Dye. *Gold Bull.* **2007**, *40*, 154–160.
31. Subramanian, V.; Wolf, E. E.; Kamat, P. V. Catalysis with TiO_2/Au Nanocomposites. Effect of Metal Particle Size on the Fermi Level Equilibration. *J. Am. Chem. Soc.* **2004**, *126*, 4943–4950.
32. Yang, L. X.; He, D. M.; Cai, Q. Y.; Grimes, C. A. Fabrication and Catalytic Properties of Co−Ag−Pt Nanoparticle-Decorated Titania Nanotube Arrays. *J. Phys. Chem. C* **2007**, *111*, 8214–8217.
33. Varghese, O. K.; Mor, G. K.; Grimes, C. A.; Paulose, M.; Mukherjee, N. A Titania Nanotube-Array Room-Temperature Sensor for Selective Detection of Hydrogen at Low Concentrations. *J. Nanosci. Nanotechnol.* **2004**, *4*, 733–737.
34. Lemon, I.; Hupp, J. T. Photochemical Quartz Crystal Microbalance Study of the Nanocrystalline Titanium Dioxide Semiconductor Electrode/Water Interface: Simultaneous Photoaccumulation of Electrons and Protons. *J. Phys. Chem.* **1996**, *100*, 14578–14580.
35. Jiang, H.; Song, H.; Zhou, Z.; Liu, X.; Meng, G. The Roles of Li^+ and F^- ions in Li-F-Codoped TiO_2 System. *J. Phys. Chem. Solids* **2007**, *68*, 1830–1835.
36. Harima, Y.; Kawabuchi, K.; Kajihara, S.; Ishii, A.; Ooyama, Y.; Takeda, K. Improvement of Photovoltages in Organic Dye-Sensitized Solar Cells by Li Intercalation in Particulate TiO_2 Electrodes. *Appl. Phys. Lett.* **2007**, *90*, 3.
37. Bahnemann, D.; Henglein, A.; Lilie, J.; Spanhel, L. Flash Photolysis Observation of the Absorption Spectra of Trapped Positive Holes and Electrons in Colloidal TiO_2. *J. Phys. Chem.* **1984**, *88*, 709–711.
38. Howe, R. F.; Graetzel, M. EPR Observation of Trapped Electrons in Colloidal TiO_2. *J. Phys. Chem.* **1985**, *89*, 4495–4499.
39. Serpone, N.; Lawless, D.; Khairutdinov, R.; Pelizzetti, E. Subnanosecond Relaxation Dynamics in TiO_2 Colloidal Sols (Particle Sizes Rp = 1−13.4 nm). Relevance to Heterogeneous Photocatalysis. *J. Phys. Chem.* **1995**, *99*, 16655–16661.
40. Vinodgopal, K.; Hua, X.; Dahlgren, R. L.; Lappin, A. G.; Patterson, L. K.; Kamat, P. V. Photochemistry of $Ru(bpy)_2(dcbpy)^{2+}$ on Al_2O_3 and TiO_2 Surfaces. An Insight into the Mechanism of Photosensitization. *J. Phys. Chem.* **1995**, *99*, 10883–10889.
41. Kongkanand, A.; Kamat, P. V. Electron Storage in Single Wall Carbon Nanotubes. Fermi Level Equilibration in Semiconductor−SWCNT Suspensions. *ACS Nano* **2007**, *1*, 13–21.
42. Fabregat-Santiago, F.; Barea, E. M.; Bisquert, J.; Mor, G. K.; Shankar, K.; Grimes, C. A. High Carrier Density and Capacitance in TiO_2 Nanotube Arrays Induced by Electrochemical Doping. *J. Am. Chem. Soc.* **2008**, *130*, 11312–11316.
43. Shankar, K.; Mor, G. K.; Prakasam, H. E.; Yoriya, S.; Paulose, M.; Varghese, O. K.; Grimes, C. A. Highly-Ordered TiO_2 Nanotube Arrays up to 220 μm in Length: Use in Water

Photoelectrolysis and Dye-Sensitized Solar Cells. *Nanotechnology* **2007**, *18*, 11.
44. Kamat, P. V.; Bedja, I.; Hotchandani, S. Photoinduced Charge Transfer between Carbon and Semiconductor Clusters. One-Electron Reduction of C_{60} in Colloidal TiO_2 Semiconductor Suspensions. *J. Phys. Chem.* **1994**, *98*, 9137–9142.
45. Redmond, G.; Fitzmaurice, D.; Graetzel, M. Effect of Surface Chelation on the Energy of an Intraband Surface State of a Nanocrystalline TiO_2 Film. *J. Phys. Chem.* **1993**, *97*, 6951–6954.
46. Ke, S. C.; Wang, T. C.; Wong, M. S.; Gopal, N. O. Low Temperature Kinetics and Energetics of the Electron and Hole Traps in Irradiated TiO_2 Nanoparticles as Revealed by EPR Spectroscopy. *J. Phys. Chem. B* **2006**, *110*, 11628–11634.
47. Berger, T.; Sterrer, M.; Diwald, O.; Knozinger, E.; Panayotov, D.; Thompson, T. L.; Yates, J. T. Light-Induced Charge Separation in Anatase TiO_2 Particles. *J. Phys. Chem. B* **2005**, *109*, 6061–6068.
48. Rajh, T.; Ostafin, A. E.; Micic, O. I.; Tiede, D. M.; Thurnauer, M. C. Surface Modification of Small Particle TiO_2 Colloids with Cysteine for Enhanced Photochemical Reduction: An EPR Study. *J. Phys. Chem.* **1996**, *100*, 4538–4545.
49. Rajh, T.; Nedeljkovic, J. M.; Chen, L. X.; Poluektov, O.; Thurnauer, M. C. Improving Optical and Charge Separation Properties of Nanocrystalline TiO_2 by Surface Modification with Vitamin C. *J. Phys. Chem. B* **1999**, *103*, 3515–3519.
50. Highfield, J. G.; Graetzel, M. Discovery of Reversible Photochromism in Titanium Dioxide Using Photoacoustic Spectroscopy. Implications for the Investigation of Light-Induced Charge-Separation and Surface Redox Processes in Titanium Dioxide. *J. Phys. Chem.* **1988**, *92*, 464–467.
51. Ramsden, J. J.; Graetzel, M. Formation and Decay of Methylviologen Radical Cation Dimers on the Surface of Colloidal CdS: Separation of Two- and Three-Dimensional Relaxation. *Chem. Phys. Lett.* **1986**, *132*, 269–272.
52. Ward, M. D.; Bard, A. J. Photocurrent Enhancement *via* Trapping of Photogenerated Electrons of TiO_2 Particles. *J. Phys. Chem.* **1982**, *86*, 3599–3605.
53. Kamat, P. V. Photoelectrochemistry in Colloidal Systems. Part 2. A Photogalvanic Cell Based on TiO_2 Semiconductor Colloid. *J. Chem. Soc., Faraday Trans. 1* **1985**, *81*, 509–518.
54. Graetzel, M.; Frank, A. J. Interfacial Electron-Transfer Reactions in Colloidal Semiconductor Dispersions. Kinetic Analysis. *J. Phys. Chem.* **1982**, *86*, 2964–2967.
55. Sodergren, S.; Siegbahn, H.; Rensmo, H.; Lindstrom, H.; Hagfeldt, A.; Lindquist, S. E. Lithium Intercalation in Nanoporous Anatase TiO_2 Studied with XPS. *J. Phys. Chem. B* **1997**, *101*, 3087–3090.
56. Erjavec, B.; Dominko, R.; Umek, P.; Sturm, S.; Pintar, A.; Gaberscek, M. Tailoring Nanostructured TiO_2 for High Power Li-ion Batteries. *J. Power Sources*, **2009**, *189*, 51−58.
57. Lindström, H.; Södergren, S.; Solbrand, A.; Rensmo, H.; Hjelm, J.; Hagfeldt, A.; Lindquist, S.-E. Li^+ Ion Insertion in TiO_2 (Anatase). 2. Voltammetry on Nanoporous Films. *J. Phys. Chem. B* **1997**, *101*, 7717–7722.
58. Wang, D. H.; Choi, D. W.; Yang, Z. G.; Viswanathan, V. V.; Nie, Z. M.; Wang, C. M.; Song, Y. J.; Zhang, J. G.; Liu, J. Synthesis and Li-Ion Insertion Properties of Highly Crystalline Mesoporous Rutile TiO_2. *Chem. Mater.* **2008**, *20*, 3435–3442.
59. Lindström, H.; Södergren, S.; Solbrand, A.; Rensmo, H.; Hjelm, J.; Hafeldt, A.; Lindquist, S.-E. Li^+ Ion Insertion in TiO_2 (Anatase). 1. Chronoamperometry on CVD Films and Nanoporous Films. *J. Phys. Chem. B* **1997**, *101*, 7710–7716.
60. Sharma, S.; Varghese, O. K.; Mor, G. K.; LaTempa, T. J.; Allam, N. K.; Grimes, C. A. Ethanol Vapor Processing of Titania Nanotube Array Films: Enhanced Crystallization and Photoelectrochemical Performance. *J. Mater. Chem.* **2009**, *19*, 3895–3898.
61. Nguyen, T. T. O.; Peter, L. M.; Wang, H. Characterization of Electron Trapping in Dye-Sensitized Solar Cells by Near-IR Transmittance Measurements. *J. Phys. Chem. C* **2009**, *113*, 8532–8536.
62. Peter, L. M. Characterization and Modeling of Dye-Sensitized Solar Cells. *J. Phys. Chem. C* **2007**, *111*, 6601–6612.
63. Bisquert, J.; Zaban, A.; Greenshtein, M.; Mora-Sero, I. Determination of Rate Constants for Charge Transfer and the Distribution of Semiconductor and Electrolyte Electronic Energy Levels in Dye-Sensitized Solar Cells by Open-Circuit Photovoltage Decay Method. *J. Am. Chem. Soc.* **2004**, *126*, 13550–13559.
64. Macak, J. M.; Gong, B. G.; Hueppe, M.; Schmuki, P. Filling of TiO_2 Nanotubes by Self-Doping and Electrodeposition. *Adv. Mater.* **2007**, *19*, 3027–3031.